FDTD Characterization of UWB Indoor Radio Channel Including Frequency Dependent Antenna Directivities

Yan Zhao, *Student Member, IEEE*, Yang Hao, *Senior Member, IEEE*, and Clive Parini, *Member, IEEE*

***Abstract*—This letter presents a modeling of ultrawideband (UWB) indoor radio channel using the finite-difference time-domain (FDTD) method. By dividing the frequency band (3–11 GHz) into eight subbands, the conventional FDTD method is applied to calculate the channel impulse responses (CIRs). At the centre frequency of each subband, measured frequency dependent dielectric constant/loss factor of different indoor materials are used and antenna patterns are taken into account by applying the equivalence principle with the total-field/scattered-field approach. Radio channel modeling results show that the base station antenna pattern variations at different frequencies can considerably influence the channel behavior in a UWB indoor environment.**

***Index Terms*—Finite-difference time-domain (FDTD), radio propagation, ray tracing (RT), ultrawideband (UWB), uniform geometrical theory of diffraction (UTD).**

I. Introduction

ULTRAWIDEBAND (UWB) communications have received great attention after the Federal Communications Commission (FCC) approved the limited use of 3.1–10.6 GHz [1]. In UWB radio channels, in addition to the distortions of multiple reflected/diffracted signals caused by the inherent material dispersion at different frequencies, the frequency selective nature of antenna radiation patterns also introduces distortions to the transmitted and received signal. Simulation models have the advantage of flexibility and convenience over measurements in terms of changing modeling environment and antenna parameters. However, conventional channel simulation tools can only be used for narrowband systems where the antenna patterns and channel parameters such as dielectric constant and conductivity are assumed constant within the operating frequency band.

Several simulation models have been proposed for UWB radio channels by applying the ray tracing (RT) technique supplemented with the uniform geometrical theory of diffraction (UTD) [2]–[4]. However, it is well known that the accuracy of RT models may decrease if small scatterers are considered in simulations or complex environment is modelled [5]. Furthermore, according to our knowledge, little attention has been paid to the influence of antenna pattern variations at different frequencies on UWB indoor radio channels. Here, we present a deterministic channel model using the finite-difference time-domain (FDTD) method [6]. Advantages of the FDTD method over RT include its capability of modeling inhomogeneous material, simultaneously providing signal coverage information throughout a given area in the time domain and its accuracy in dealing with small areas and small scatterers. Although the dispersive FDTD has been developed to model general dispersive materials, the determination of the coefficients for the rational functions to fit measurement data requires further effort such as applying the Padé approximations or the frequency-domain prony method (FDPM) [7], [8]. Also the inclusion of frequency dependent antenna pattern in time domain dispersive FDTD model may increase storage and computation requirement. In this letter, the conventional FDTD method is applied with a subband approach to the modeling of UWB indoor radio channel.

Manuscript received August 11, 2006; revised January 9, 2007.

The authors are with the University of London, London E1 4NS, U.K. (e-mail: y.hao@elec.qmul.ac.uk).

Digital Object Identifier 10.1109/LAWP.2007.891963

II. The FDTD Radio Channel Model

The subband FDTD method has been proposed in [9] and [10], where the choice on the number of subbands is also analyzed. For the subband FDTD model used in this letter, in order to take into account the antenna pattern variations as well as the material dispersions at different frequencies, the whole UWB is divided into eight subbands with 1 GHz bandwidth. Each subband is simulated separately and a combination technique is used to recover the overall channel impulse response (CIR) [9], [10]. At each subband, the frequency dependent material properties are obtained from measurement [11]. The complex Gaussian monocycles with different pulse width are used for the excitation signal according to the centre frequency of each subband.

The antenna patterns are taken into account in the FDTD channel model by applying the equivalence principle [12] with the total-field/scattered-field approach. Two different UWB antennas are used to model the basestation antenna: the printed horn-shaped self-complementary antenna (HSCA) and the planar inverted cone antenna (PICA) [13]. The antennas are simulated using CST Microwave Studio [14] and validated by measurement. The antenna patterns for applying the equivalence principle can be obtained from either measurement or simulations. The complex radiated electric far-field patterns on the H-plane (the dominant plane) for both antennas are calculated from numerical simulations at the centre frequency of each subband. The equivalent surface (Huygen's surface) can be any shape dividing two domains. However, in order to avoid the staircase approximations of curved structures in

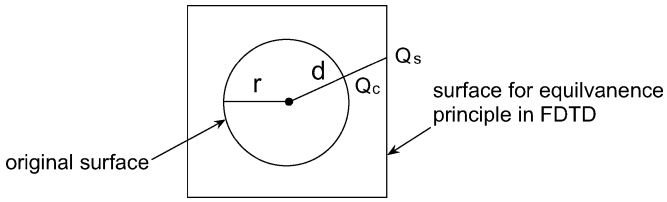

Fig. 1. Demonstration of the original circular surface where the antenna radiation patterns are calculated and the square surface for applying the equivalence principle in FDTD mesh. Q_c and Q_s are the example field points where the transformation is performed.

the FDTD grid, a square surface in two-dimensions (2-D) or a cubic surface in three-dimensions (3-D) may be used. For a 2-D case, since the original radiation patterns are calculated on a circular surface, the field at any point on a concentric square surface needs to be transformed from the corresponding point on the circular surface (Fig. 1) using

$$E_s = E_c \frac{\sqrt{r}}{\sqrt{d}} e^{-j\frac{2\pi f}{c}(d-r)} \tag{1}$$

where E_s is the electric field at a point on a concentric square surface (outside the circular one), d is the distance from the point to the center of the square surface, E_c is the electric field at the corresponding point on the circular surface with radius r, f is the frequency at which the antenna pattern is transformed, and c is the speed of wave propagation.

Only the scattered field is calculated inside the surface to allow the scattering from surrounding medium, and the total field is calculated elsewhere. This satisfies the equivalence principle where the current source can only radiate towards outside the surface. In order to validate the equivalence current model, the radiated electric field pattern from the current surface is calculated on a circular surface (outside the square one) from FDTD iterations and compared with the original antenna patterns used as source excitations at different subband frequencies. Fig. 2 shows the comparison between the antenna patterns directly calculated from CST by modeling the actual antenna and the patterns calculated from FDTD applying the equivalence principle at the centre frequencies of the first subband (3.5 GHz) and the eighth subband (10.5 GHz). It can be seen that at lower frequencies, both PICA and HSCA have omnidirectional radiation patterns while at higher frequencies, the radiation pattern of HSCA has severer distortions compared with PICA.

III. Numerical Results

Simulations are carried out in 2-D with the transverse magnetic (TM) polarized field is considered. As shown in Fig. 3, a small office is modelled with the dimensions are given in the figure. For all the subband simulations, the FDTD cell size is $\Delta x = \Delta y = 3.0 \times 10^{-3}$ m with the time step $\Delta t = 7.0 \times 10^{-12}$ s according to the stability criterion [6]. A 10-cell Berenger's perfectly matched layer (PML) is used to truncate the simulation domain [15]. The directions of radiated field are indicated by the coordinates shown in both Figs. 2 and 3.

Fig. 4 shows the time domain CIRs at 3 m to the transmitter at different subbands. It clearly shows that the CIRs are considerably different at different subbands, which is caused by both the change of channel behavior introduced by the material dispersions, and the antenna pattern variations at different frequencies. Comparing the first received pulse [line-of-sight (LOS) path], the variation of signal amplitude using PICA as base station antenna is less significant compared with HSCA, which is in accordance with the fact that the PICA exhibits relatively more stable radiated field across the whole frequency band [13]. Table I lists the detected number of multipath components (MCs) using different base station antennas at different subbands. For comparison, simulation is also carried out using a point source (PS) as an ideally omnidirectional base station antenna at all subbands. For the ideal PS case, at lower frequencies, the overlapping of multipath signals causes the small number of detected MCs; while at higher frequencies, the effect of multipath interference becomes less due to the short duration of the transmitted

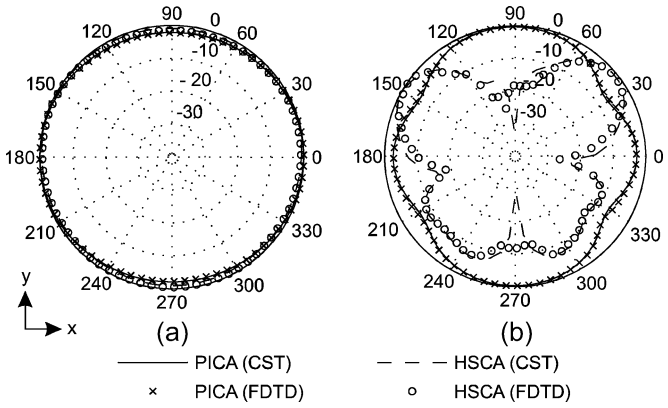

Fig. 2. Comparison of normalized E-field radiation patterns of PICA and HSCA at (a) 3.5 and (b) 10.5 GHz calculated from CST microwave studio modeling the actual antenna and from FDTD applying the equivalence principle.

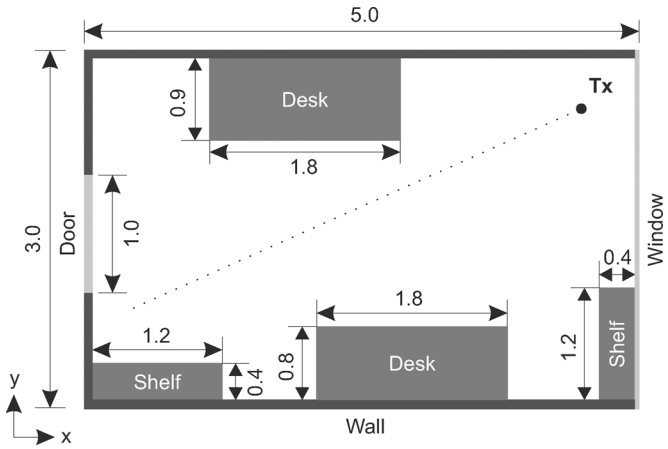

Fig. 3. Layout of the subband FDTD simulation domain (unit: m).

TABLE I
Number of MCs at Different Subbands Using PICA, HSCA, and PS as Base Station Antennas, Respectively

Sub-band No.	1	2	3	4	5	6	7	8
No. of MCs (PICA)	13	15	14	12	11	16	16	17
No. of MCs (HSCA)	11	7	12	13	15	11	13	13
No. of MCs (PS)	10	13	13	14	15	17	17	18

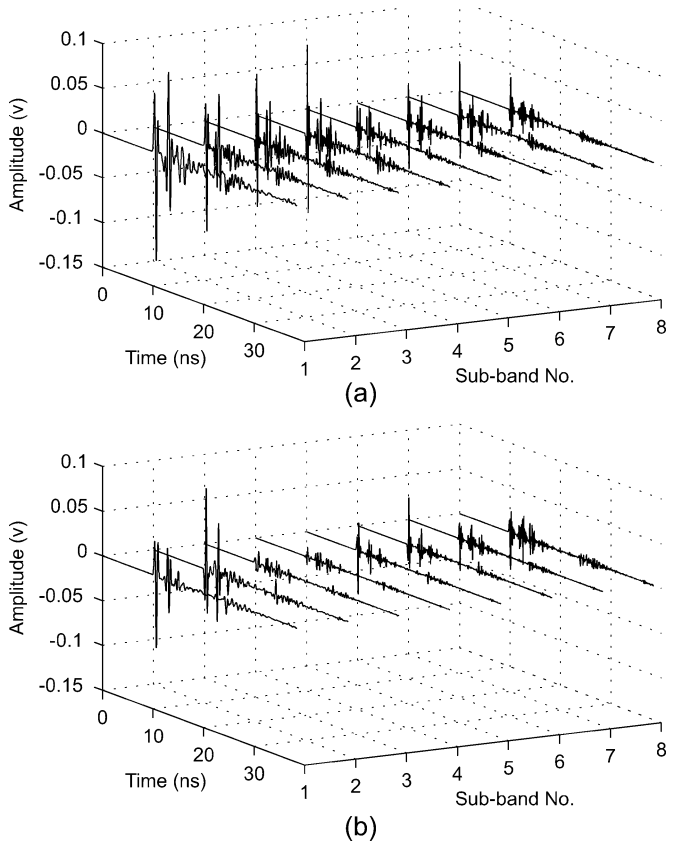

Fig. 4. Time domain CIRs at 3 m to Tx at different subbands using (a) PICA and (b) HSCA as base station antennas.

pulse. Compared with the PS case, the result from PICA shows its relatively stable omnidirectional radiation property; while for HSCA, the pattern distortions at higher frequencies (sixth, seventh, and eighth subband) reduces the number of MCs, which is in agreement with [16] that the omnidirectional base station antenna causes more MCs to be captured at the receiver.

The power delay profiles (PDPs) for different basestation antennas are calculated from the combined time domain signal. Fig. 5 shows the PDPs at 3 m to the transmitter and a threshold of -23 dB for detecting the MCs. It can be seen that the PDP with PICA as base station antenna contains more MCs compared with HSCA, which indicates that the pattern distortions at higher frequencies can cause the overall reduction of the number of received MCs.

The path loss is calculated along the dotted line from 1 to 5 m to the transmitter as shown in Fig. 3. Then a least square fitting method is used to extract the path loss exponent γ. Fig. 6 shows the calculated path loss at different Tx-Rx separations for different base station antennas. The values of path loss exponent are relatively low due to the multiple reflections in the small office environment. Table II lists the values of the path loss exponent from simulations using different base station antennas, and measurement with omni/omni and omni/dir antenna combinations [16]. It can be seen that in small indoor environments, our simulation results are close to measurement. It is also found that the path loss exponent for HSCA is slightly higher than that for

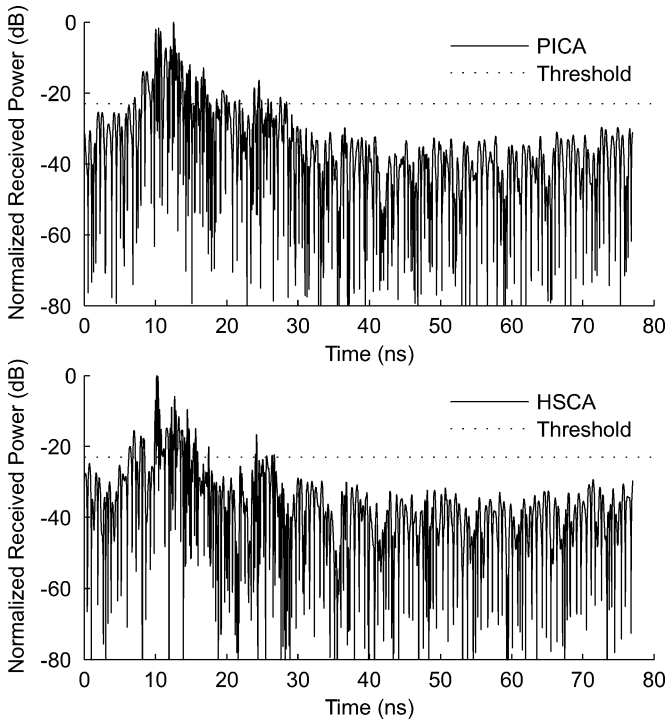

Fig. 5. PDPs calculated from combined time domain CIRs at 3 m to Tx for different base station antenna cases. A threshold of -23 dB for detecting the MCs is also shown.

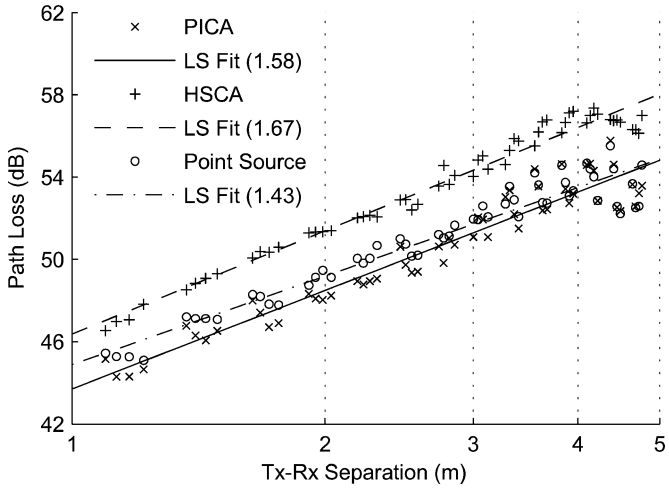

Fig. 6. Path loss at 1 to 5 m to the transmitter for different base station antenna cases. The least square (LS) fitted lines and the values of path loss exponent (in brackets) are also shown.

TABLE II
PATH LOSS EXPONENT, γ CALCULATED FROM SIMULATIONS USING DIFFERENT BASE STATION ANTENNAS AND MEASUREMENTS

	Simulation			Measurement	
Antenna	PICA	HSCA	PS	Omni/Omni	Omni/Dir
γ	1.58	1.67	1.43	1.55	1.65

PICA, which is caused by the smaller number of received MCs when using HSCA as base station antenna.

The root-mean-square (rms) delay spread is important for wireless system design since it indicates the dispersion of a

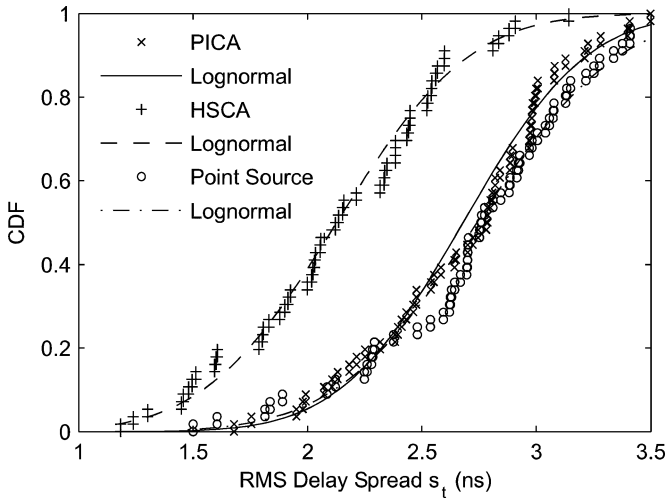

Fig. 7. CDF of rms delay spread for using PICA, HSCA, and PS as base station antennas, respectively.

TABLE III
THE MEAN, MINIMUM, AND MAXIMUM VALUES OF RMS DELAY SPREAD, σ_τ FOR DIFFERENT BASE STATION ANTENNAS

Antenna	$\sigma_{\tau,mean}$ (ns)	$\sigma_{\tau,min}$ (ns)	$\sigma_{\tau,max}$ (ns)
PICA	7.36	2.82	12.24
HSCA	4.73	1.40	9.87
PS	7.74	2.25	14.17

radio channel. It can be calculated from the PDPs with a proper threshold. For our case, the PDPs are taken at various locations along the dotted line from 1 to 5 m to the transmitter as shown in Fig. 3 in order to calculate the RMS delay spread. The cumulative distribution function (CDF) is then calculated from the obtained data set. It is shown in Fig. 7 that the simulation results are in good agreement with the lognormal distribution for all basestation antenna cases. The close match of the results from PICA and PS as base station antennas proves that PICA has relatively stable omnidirectional radiation properties at UWB frequencies. Table III lists the mean, minimum, and maximum values of the RMS delay spread of our model (Fig. 3) for different base station antenna cases. When the HSCA is used in contrast to PICA, the mean, minimum, and maximum rms delay spread are decreased by 35.7%, 50.4%, and 19.4%, respectively.

IV. CONCLUSION

This letter presents an investigation of the impact of frequency dependent antenna patterns on UWB indoor radio channel using the FDTD method. By dividing the frequency band into eight subbands, both the material dispersion effect and frequency-dependent antenna directivities are taken into account in FDTD simulations. Two different antennas are considered for base station antenna modeling by applying the equivalence principle: PICA and HSCA, which have different radiation pattern variations across the UWB frequency band. UWB indoor radio channel modeling results show that the antenna pattern distortions at higher frequencies can cause the reduction of the number of received MCs, leading to the increase of path loss exponent. Meanwhile, the reduction of rms delay spread is also obtained when using HSCA as the base station antenna.

Previous studies demonstrate that the magnitude of the antenna transfer function should be invariable or flat within UWB frequency band [17], in other words, the radiation patterns of UWB antennas should be stable at different frequencies in order to minimize the distortion of transmitted signal. However, the reduction of rms delay spread is also a desired feature to mitigate the multipath effect in wireless radio channels. Therefore cares must be taken for the frequency dependent antenna performance when designing UWB wireless radio systems.

REFERENCES

[1] Revision of Part 15 of the Commission's Rules Regarding Ultra-Wide-Band Transmission Systems Federal Commun. Comm., First Rep. Order ET Docket 98-153, Feb. 2002.
[2] A. M. Attiya and A. Safaai-Jazi, "Simulation of ultra-wideband indoor propagation," *Microw. Opt. Technol. Lett.*, vol. 42, no. 2, 2004.
[3] B. Uguen, E. Plouhinec, Y. Lostanlen, and G. Chassay, "A deterministic ultra wideband channel modelling," in *IEEE Conf. Ultra Wideband Syst. Technol.*, May 2002.
[4] F. Tehoffo-Talom, B. Uguen, E. Plouhinec, and G. Chassay, "A site-specific tool for UWB channel modeling," in *Joint UWBST IWUWBS Int. Workshop on Ultra Wideband Syst. Technol.*, May 2004.
[5] K. A. Remley, H. R. Anderson, and A. Weisshar, "Improving the accuracy of ray-tracing techniques for indoor propagation modelling," *IEEE Trans. Veh. Technol.*, vol. 49, no. 6, 2000.
[6] A. Taflove, *Computational Electrodynamics: The Finite Difference Time Domain Method*. Norwood, MA: Artech House, 1995.
[7] W. H. Weedon and C. M. Rappaport, "A general method for FDTD modelling of wave propagation in arbitrary frequency dispersive media," *IEEE Trans. Antennas Propag.*, vol. 45, no. 3, 1997.
[8] G. X. Fan and Q. H. Liu, "An FDTD algorithm with perfectly matched layers for general dispersive media," *IEEE Trans. Antennas Propag.*, vol. 48, no. 5, 2000.
[9] Y. Zhao, Y. Hao, and C. G. Parini, "Two novel FDTD based UWB indoor propagation models," in *Proc. 2005 IEEE Int. Conf. Ultra-Wideband*, Sep. 2005.
[10] Y. Zhao, Y. Hao, A. Alomainy, and C. G. Parini, "UWB on-body radio channel modelling using ray theory and subband FDTD method," *IEEE Trans. Microw. Theory Tech.*, vol. 54, no. 4, pp. 1827–1835, Apr. 2006.
[11] A. Safaai-Jazi, S. M. Riad, A. Muqaibel, and A. Bayram, "Ultra-wideband propagation measurements and channel modelling," Rep. Through-the-Wall Propag. Mater. Characteriz. Nov. 2002.
[12] L. Talbi, "Simulation of indoor UHF propagation using numerical technique," in *Proc. Canad. Conf. Elect. Comput. Eng.*, May 2001.
[13] A. Alomainy, Y. Hao, C. G. Parini, and P. S. Hall, "Comparison between two different antennas for UWB on-body propagation measurements," *IEEE Antennas Wireless Propag. Lett.*, vol. 4, pp. 31–34, 2005.
[14] *"CST Microwave Studio, User's Manual,"* ver. 2006.
[15] J. R. Berenger, "A perfectly matched layer for the absorption of electromagnetic waves," *J. Computat. Phys.*, vol. 114, pp. 185–200, Oct. 1994.
[16] J. A. Dabin, N. Nan, A. M. Haimovich, E. Niver, and H. Grebel, "The effects of antenna directivity on path loss and multipath propagation in UWB indoor wireless channels," in *Proc. 2003 IEEE Conf. Ultra Wideband Syst. Technol.*, Nov. 2003.
[17] Z.-N. Chen, X.-H. Wu, H.-F. Li, N. Yang, and M. Y. W. Chia, "Considerations for source pulses and antennas in UWB radio systems," *IEEE Trans. Antennas Propag.*, vol. 52, no. 7, Jul. 2004.